Magnetic phase diagram of magnetoelectric $CuFeO_2$ in high magnetic fields

G. Quirion and M. L. Plumer
Department of Physics and Physical Oceanography, Memorial University, St. John's, Newfoundland, Canada A1B 3X7

O. A. Petrenko and G. Balakrishnan
Department of Physics, University of Warwick, Coventry CV4 7AL, United Kingdom

C. Proust
Laboratoire National des Champs Magnétiques Intenses (CNRS), 31400 Toulouse, France
(Received 25 May 2009; revised manuscript received 4 August 2009; published 26 August 2009)

A series of ultrasonic velocity measurements using both high-field pulsed and conventional superconducting magnets were used to determine the magnetic phase diagram of magnetoelectric $CuFeO_2$ up to 53 T. The results clearly indicate a previously undetected transition at about 49 T below 10 K. Analysis of Landau-type free energy suggests that this new phase boundary is due to a spin-flop transition.

DOI: 10.1103/PhysRevB.80.064420 PACS number(s): 75.30.Kz, 75.80.+q, 64.60.−i, 62.20.de

I. INTRODUCTION

Magnetic field-temperature phase diagrams often reveal useful information on fundamental magnetic interactions in complex spin systems and have been studied extensively in a variety of multiferroic compounds.[1–3] In addition to the intrinsic scientific interest in the coupling between magnetic and electric degrees of freedom, the potential for technological applications has fueled intense activity into an increasing number of magnetoelectric compounds.[4–7] A characteristic feature of systems such as $RMnO_3$,[8] $Ni_3V_2O_8$,[9] $CuFeO_2$,[10] and $BiFeO_3$ (Ref. 11) is that magnetic frustration, caused by competing interactions or frustrated antiferromagnetic coupling on a triangular lattice, leads to many exotic spin configurations which are responsible for magnetoelectric coupling.

The focus of the present work is on the high-field magnetic properties of the geometrically frustrated antiferromagnet $CuFeO_2$. In this compound, the Fe^{3+} ions form ABC stacked triangular layers and exhibit a rhombohedral $R\bar{3}m$ crystal structure at high temperature. The application of a magnetic field up to 23 T along the c axis has revealed a complex series of low-temperature magnetic phase transitions determined by magnetization, heat capacity, and neutron diffraction measurements.[10,12–14] The magnetic phase diagram has been extended up to 43 T using pulsed high magnetic fields,[15,16] complementing earlier magnetization data at low temperature in fields up to 100 T.[17] In zero magnetic field, there is an incommensurate (IC) linearly polarized spin structure characterized by a polarization vector $\mathbf{S}\|\hat{\mathbf{c}}$ below $T_{N1}\simeq 13.7$ K. With decreasing temperature, a first-order transition is observed at $T_{N2}\simeq 10.6$ K to a period-4 ($\uparrow\uparrow\downarrow\downarrow$) basal-plane modulated commensurate (C) ordering, again with $\mathbf{S}\|\hat{\mathbf{c}}$.[18] The application of a magnetic field along the c axis stabilizes a series of different IC and C spin structures. Some of these have been characterized by comparing the plateaus observed in magnetization data to the saturation value.[17,19] These field-induced spin configurations have been described as follows: a noncollinear IC structure for 7 T $<$H$<$ 13 T (the only magnetoelectrically active phase), a period-5 ($\uparrow\uparrow\uparrow\downarrow\downarrow$ with $\mathbf{S}\|\hat{\mathbf{c}}$) collinear state for 13 T$<$H$<$20 T, a period-3 ($\uparrow\uparrow\downarrow$ with $\mathbf{S}\|\hat{\mathbf{c}}$) collinear structure for 20 T$<$H$<$34 T, followed by a period-3 canted spin configuration. A transition to the paramagnetic state has been speculated to occur above 70 T at low temperature.[15] Neutron diffraction measurements have verified only the lower-field period-4, IC and period-5 phases.

It has been emphasized that one can expect the absence of typical spin-orbit mechanisms since $L=0$ is associated with the $S=5/2$ Fe^{3+} ions in $CuFeO_2$.[14,16,20] The stability of states with $\mathbf{S}\|\hat{\mathbf{c}}$ up to 43 T is thus quite remarkable in the absence of strong single-ion (or exchange) axial anisotropy, as allowed by crystal symmetry. Nonfrustrated, as well as frustrated triangular antiferromagnets, with weak axial anisotropy such as $CsNiCl_3$ are expected to exhibit a low-field (at a few tesla) spin-flop transition.[21,22] The stability of field-induced collinear states in $CuFeO_2$ has been linked to magnetoelastic coupling, which is known to be strong in this compound.[19,23–26]

A number of Ising-based models have been proposed which yield a large number of possible commensurate collinear states at low temperature in an applied magnetic field for triangular antiferromagnets. These include effects of up to third-neighbor in-plane exchange interactions,[17,27,28] as well as those from magnetoelastic driven biquadratic exchange.[29] Even if these models account for many of the collinear states observed in $CuFeO_2$, they cannot be used to describe other exotic states which are due to competitive interactions. Heisenberg models with small axial anisotropy which also include interplane exchange interactions have also been analyzed.[14,29,30] Additional magnetoelectric coupling effects giving rise to antisymmetric exchange were shown to stabilize the noncollinear IC phase.[31] Based on this latter spin Hamiltonian, a Landau-type model was proposed, that includes a trigonal anisotropy term, which reproduces essential features of the lower-field regions of the H-T phase diagram as well as the magnetoelectric effect in this compound.[32]

Motivated by the absence of detailed data in the field region above 43 T, as well as the existence of strong spin-lattice coupling in this compound, we performed ultrasound

velocity measurements on $CuFeO_2$ as a function of temperature and magnetic field up to 53 T. Below 40 T, the observed anomalies coincide well with the established phase diagram. At higher fields, a new phase transition is clearly observed at 49 T. The previous models described in Refs. 31 and 32 are extended to higher field values where a spin-flop transition, involving a period-3 phase, is found.

The remainder of the paper is organized as follows. We briefly describe the experimental methods in Sec. II, while ultrasonic velocity data as a function of temperature and magnetic field are presented in Sec. III. The results of a numerical analysis of the nonlocal Landau-type free-energy functional at high field are presented in Sec. IV. A final discussion and conclusions are made in Sec. V.

II. ULTRASOUND AT HIGH FIELDS

All data were collected using $CuFeO_2$ single crystals grown with an infrared image furnace.[13] For the ultrasound velocity experiments, several samples were prepared with polished parallel faces normal to the principal crystallographic directions. Samples were roughly cubic in shape with edges of approximately 3 mm in length. Measurements were done using exclusively longitudinal modes, propagating along the threefold symmetry c axis or along the twofold symmetry, referred as the z and x axis, respectively. In both cases, plane waves were generated and detected using 30 MHz $LiNbO_3$ transducers bonded on opposite faces of the sample. The normalized velocity variation $(\Delta v/v)$ was obtained using two different pulsed heterodyne phase sensitive spectrometers. For high-field experiments in Toulouse, a spectrometer[33] was specially adapted for ultrasound measurements in pulsed magnetic fields up to 53 T with a typical rising time of 50 and 250 ms for the down field time. As in the usual ultrasonic setup, based on the echo method, a pulse of sound in the 30–600 MHz range is sent to a sample. One of the particularities here is that a higher repetition rate of 100 kHz is used. A higher repetition rate is necessary in order to guarantee that the variation of the magnetic field between two successive pulses is small. A phase comparator coupled with a constant phase-limiting amplifier is used for the sound velocity measurement while the data acquisition is achieved with a Lecroy oscilloscope in a sequential mode. Finally, for comparison and calibration purposes, additional experiments at lower magnetic fields were also performed up to 10 T using another high resolution spectrometer in conjunction with a conventional DC superconducting magnet.

III. SOUND VELOCITY DATA

In Fig. 1 we present the low-temperature dependence of the normalized velocity variation of longitudinal modes propagating along the c axis $(\Delta v/v_{Lz})$ and x axis $(\Delta v/v_{Lx})$. All measurements were made with a constant magnetic field applied along the c axis. The zero-field data, previously analyzed using a Landau-type model,[25,26] indicate that the anomaly observed at $T_{N1} \simeq 13.7$ K is associated with the softening of a E-symmetric mode leading to a *pseudoproper ferroelastic* structural phase transition. As the soft mode

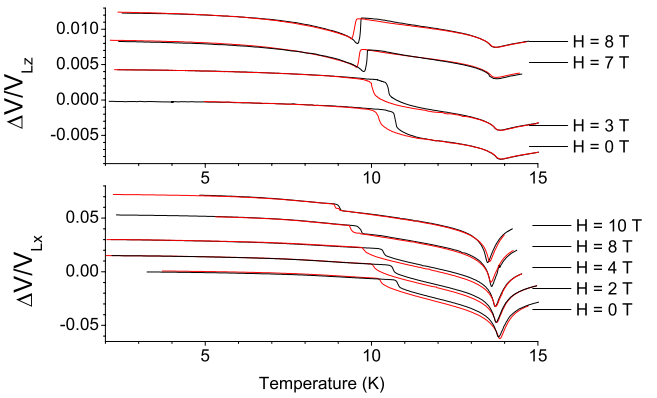

FIG. 1. (Color online) Temperature dependence of the normalized velocity variation of longitudinal waves propagating along c $(\Delta V/V_{Lz})$ and x axis $(\Delta V/V_{Lx})$. Curves in black/red correspond to increasing/decreasing temperature sweeps.

couples with the z component of the local magnetic moments, the magnetic phase transition coincides with the structural one. The analysis also shows that the second anomaly is a result of a period-4 umklapp term which accounts for the first-order character of the magnetic transition at $T_{N2} \simeq 10.6$ K. As a magnetic field is applied along the z direction, we notice in Fig. 1 that both critical temperatures T_{N1} and T_{N2} shift to lower temperatures, in good agreement with the previously determined low-field phase diagram of $CuFeO_2$.[10,13] Results for $\Delta v/v_{Lz}$ also show a particular behavior for fields larger than 7 T. Above that critical field, the velocity displays a sudden drop at T_{N2} rather than the noticeable rapid rise at lower fields. This change in the temperature dependence of v_{Lz} around T_{N2}, with no significant change on v_{Lx}, is more likely attributed to the noncollinear-incommensurate spin configuration which is known to stabilize between 7 and 13 T.[10,13]

Over the years, high pulsed magnetic field facilities have developed experimental systems which now allow the measurement of sound velocity. This approach, especially sensitive to spin-lattice coupling, has proven very useful in the characterization of magnetic transitions in a variety of systems.[33–38] Due to short rising time associated with pulsed field magnets, these velocity experiments are generally performed by measuring the phase difference between a reference signal and that of an echo. In a typical transmission configuration, the phase difference for the nth echo is simply given by

$$\phi = 2\pi f \tau = \frac{(2n-1)2\pi f l}{v_s}, \tag{1}$$

where v_s is the sound velocity at frequency f, while τ is the echo time of flight for a sample of length l. As the frequency is kept constant during the experiment, we obtain that the phase variation

$$\Delta\phi = -\frac{(2n-1)2\pi f l}{v_s}\frac{\Delta v_s}{v_s} \tag{2}$$

can be related to the normalized velocity variation $\frac{\Delta v_s}{v_s}$.

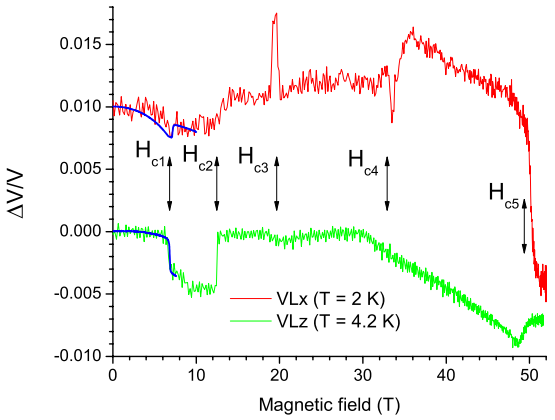

FIG. 2. (Color online) Field dependence of the normalized velocity variation of longitudinal waves propagating along the x axis (V_{Lx}) and c axis (V_{Lz}). The continuous blue curves represent data collected using a quasistatic field produced by a conventional superconducting magnet up to 10 T.

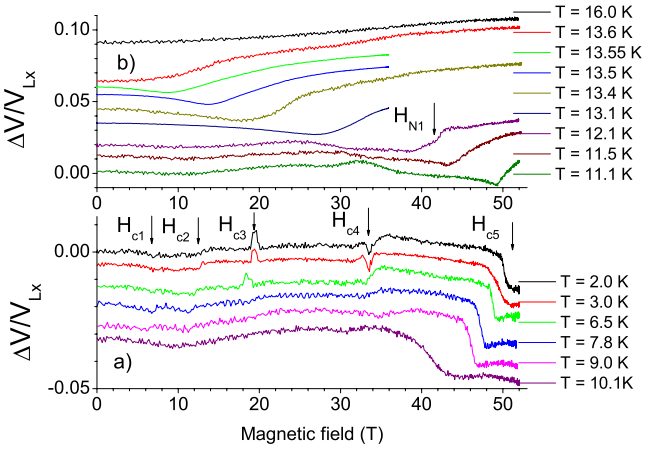

FIG. 3. (Color online) Field dependence of the normalized velocity variation of longitudinal waves propagating along the x axis. For clarity, results obtained below and above $T_{N2} \sim 10.6$ K are presented separately.

In an attempt to test if our high-field results reveal the true equilibrium properties, we compare in Fig. 2 data collected using a conventional superconducting magnet with those obtained with a short rising time pulsed magnet. For this comparison, the phase data (high field) have been scaled [Eq. (2)] to match the low-field velocity measurements (continuous curves up to 10 T). As shown in Fig. 2, results obtained with both experimental setups agree well, with no significant heating effect due to induction as $CuFeO_2$ is a poor electrical conductor.

This comparison allows us to determine, with confidence, the actual velocity variations at high field which shows five distinct concurrent anomalies on V_{Lx} and V_{Lz}. Critical fields associated with these anomalies correspond to $H_{c1} \sim 7$ T, $H_{c2} \sim 12.5$ T, $H_{c3} \sim 19$ T, $H_{c4} \sim 32$ T, and $H_{c5} \sim 49$ T. The first four critical fields agree well with anomalies observed on high-field x-ray diffraction and magnetization measurements.[15,19] More importantly, the pronounced anomalies visible on V_{Lx} and V_{Lz} around 49 T corresponds to a new phase transition, not detected in previous high-field investigations.

We show in Figs. 3 and 4 a series of high-field measurements at different temperatures. For clarity, data for temperatures below and above T_{N2} are presented in (a) and (b), respectively. Between T_{N2} and T_{N1} only one anomaly is observed on V_{Lx} [Fig. 3(b)] with no significant variation visible on V_{Lz} [Fig. 4(b)]. These results are compared to the magnetoelastic variation measured in the paramagnetic phase at 16 K. Based on this comparison, the observed anomaly on V_{Lx} can be associated with the IC-paramagnetic phase transition (H_{N1}). Below T_{N2}, both sets of measurements reveal five distinct anomalies marked by arrows and labeled H_{C1} to H_{C5}.

Using the determined critical fields, we present in Fig. 5 the magnetic phase diagram of $CuFeO_2$ up to 53 T for a field applied along the c axis. Contrary to the phase diagram proposed by Terada *et al.*,[15] which shows five phases at 0 K, our sound velocity data reveal an additional phase boundary at 49 T. Fitting of the temperature dependence of H_{N1} (continuous curve), using a mean field extrapolation $H_{N1} \sim \sqrt{T_{N1} - T}$, leads to an upper critical field of 83 T at 0 K. This value agrees reasonably well with the saturation field (~70 T) determined from magnetization measurements.[17]

IV. MODEL RESULTS AT HIGH FIELD

Previously described models based on a spin Hamiltonian, which includes up to third-neighbor in-plane and first-neighbor interplane isotropic exchange interactions, uniaxial anisotropic exchange, biquadratic symmetric exchange (from magnetoelastic coupling), and biquadratic antisymmetric exchange (from magnetoelectric coupling), were applied to $CuFeO_2$ at zero temperature[31] and extended to finite temperature through a nonlocal Landau-type free energy.[32] In the latter study, an additional trigonal anisotropy term was shown to cant the noncollinear spin configuration and thus giving rise to an induced electric polarization. In theses studies, the magnetic field was restricted to only moderately large values. We extend here these models to higher field in order

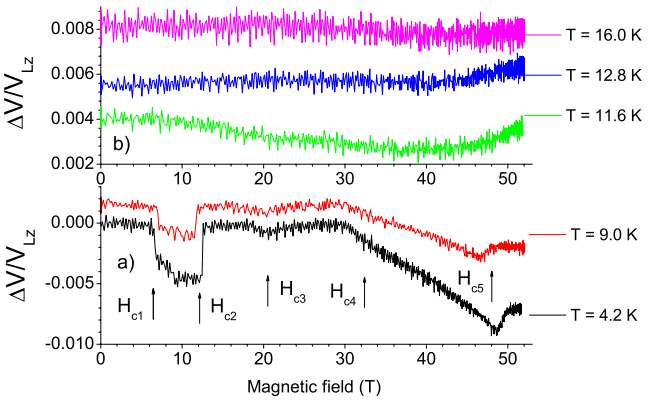

FIG. 4. (Color online) Field dependence of the normalized velocity variation of longitudinal waves propagating along the c axis. For clarity, results obtained below and above $T_{N2} \sim 10.6$ K are presented separately.

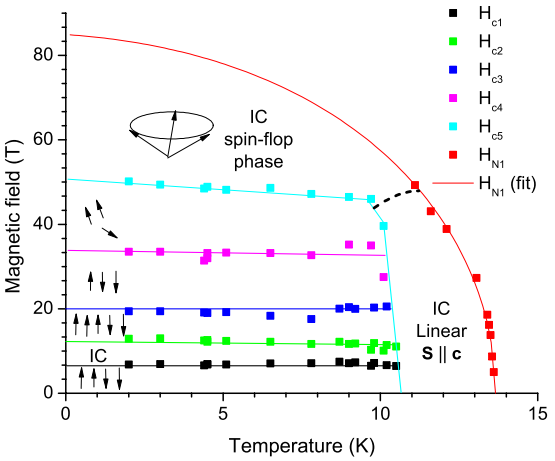

FIG. 5. (Color online) Magnetic phase diagram of $CuFeO_2$. The lines are guides for the eyes, while the boundary for the critical field H_{N1} (red curve) is obtained by fitting the experimental data point using a mean field prediction. The arrows represent the proposed spin configurations. The broken line represents results from Landau theory.

to identify the spin configuration observed above 49 T.

Consider first the zero temperature model of Ref. 31. The energy of a variety of commensurate phases were compared with increasing magnetic field (H) applied along the c axis. Incommensurate states require some care to simulate in this finite-sized system. Using estimates for the magnitude of the near-neighbor in-plane exchange interaction J_1, it was concluded that a multiplication factor of 5.6 T should approximately correspond to the real applied field strength. Using this factor, the predicted transitions were consistently somewhat smaller than the observed values. For fields larger than the model field value $H \simeq 3$, the spin state with a period-3 modulation in the basal plane, and alternating spins between planes, (3,1), gives the minimum energy. At about $H \simeq 4.5$, a change of slope is observed in the plot of M_z vs H which was attributed to a transition from the state with $\mathbf{S} \| \hat{\mathbf{c}}$ to a canted period-3 phase.

Figure 6 also shows new $T=0$ model results for M_z vs H of the (3,1) state at higher field values using the same parameters as in Ref. 31. There appears to be a plateau in the region of $H \simeq 7.5$ suggestive of a transition to another phase. This corresponds to a real field of about 40 T. This value is somewhat lower than the new transition line observed in Fig. 5, consistent with previous correlations between model and experimental phase boundaries.

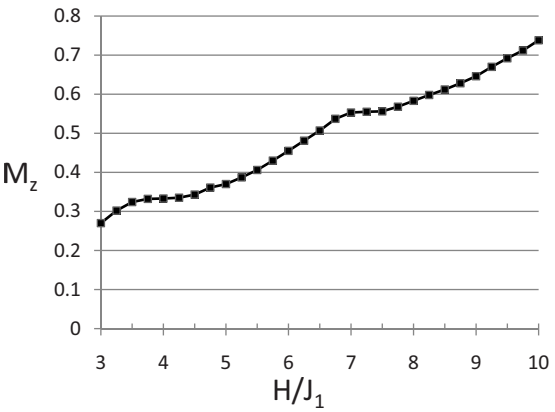

FIG. 6. Field dependence (H/J_1) of the magnetization M_z calculated at 0 K for the (3,1) commensurate state.

In addition, a new analysis was made of the Landau model at fields higher than the region $H=0$ to $H=5$ considered in Ref. 32. In this theory, the free energy is expressed as an expansion (to sixth order) in powers of the spin density,

$$\boldsymbol{\rho}_j(\mathbf{r}) = \mathbf{m} + \mathbf{S}_j e^{i\mathbf{Q}\cdot\mathbf{r}} + \mathbf{S}_j^* e^{-i\mathbf{Q}\cdot\mathbf{r}}, \tag{3}$$

where j labels the three ABC stacked triangular planes. As a finite expansion in the field-induced magnetization m and the polarization vector $\mathbf{S}$ (which is also the long range order parameter), Landau theory is strictly applicable in regimes of the phase diagram where these quantities are not too large. This implies that the model may be inappropriate at small T and also at large H. However, entire experimental phase diagrams can be successfully reproduced by the Landau approach, even as an expansion to only fourth order.[22] We restrict the analysis here to regions of the phase diagram close to the paramagnetic phase boundary where S is small. Although the model, using parameters as in Ref. 32, does not yield a canted period-3 phases, below $T \simeq 1.4$ there is a clear spin-flop transition at about $H \simeq 6$ from a collinear period-3 state with $\mathbf{S} \| \hat{\mathbf{c}}$ to a noncollinear IC state (which is close to period-3) having $\mathbf{S} \perp \hat{\mathbf{c}}$. This describes a slightly incommensurate version of the classic 120° spin structure.[22] At lower temperatures, this transition boundary increases and appears to asymptotically approach a low-T value close to 7, as found in the zero-field model analysis. There is also a new phase-boundary region between the IC collinear low-field, high-T $\mathbf{S} \| \hat{\mathbf{c}}$ phase, to the new IC spin-flop phase where $\mathbf{S}$ rotates continuously over a very small field region ($\Delta H \simeq 0.1$) from parallel to perpendicular to the c axis. This region is indicated by the broken line in Fig. 5.

Spin-flop transitions are generic to easy axis antiferromagnets and arise due to a simple competition between low order anisotropy (of single-ion or, as in the present case, exchange in origin) $-J_z|S_z|^2$ and higher-order terms in the Landau free energy of the form[32] $[2B_4 + \frac{1}{6}C(m^2 + 2|S|^2)]|\mathbf{m}\cdot\mathbf{S}|^2$. In the case $\mathbf{m} \| \mathbf{H} \| \mathbf{z}$, the transition occurs at $[2B_4 + \frac{1}{6}C(m^2+2|S|^2)]m^2 = J_z$. Temperature dependence of the phase boundary enters through $|\mathbf{S}|^2$. A large spin-flop field can occur in such a model if $B_4 < 0$, which is a consequence of the fitting procedure described in Ref. 32 and is likely due to strong magnetoelastic coupling.

V. DISCUSSION AND CONCLUSIONS

In summary, high-field ultrasonic velocity measurements have been used to determine the magnetic phase diagram of $CuFeO_2$ up to 53 T. Anomalies observed in the field dependence of the velocity of longitudinal modes propagating along x and c agree well with magnetization changes observed up to 40 T.[19] In addition, our measurements reveal a new phase transition clearly visible around 49 T at low temperatures (below $T_{N2} \sim 11$ K). After a close inspection of magnetization measurements realized up to 100 T on a pow-

der sample,[17] it seems that the strong anomaly observed at 49 T on the velocity coincides well with a small feature visible on the field derivative of the magnetization. Analysis based on an extended version of a Landau model previously used to account for the series of magnetic states observed in $CuFeO_2$ suggests that the new phase transition could be from a canted period-3 phase to a noncollinear IC state with $\mathbf{S} \perp \hat{\mathbf{c}}$. This new spin configuration would correspond to an incommensurate version, close to a period-3, of the classic 120° spin structure normally observed in triangular based frustrated antiferromagnets such as $CsNiCl_3$ and $CsMnBr_3$.[39] This phase would also be consistent with a magnetization value that increases gradually up to the saturation value measured above 70 T.[17] It should also exhibit an induced electric polarization through the coupling term discussed in Ref. 10.

ACKNOWLEDGMENTS

This work was supported by grants from the Natural Science and Engineering Research Council of Canada (NSERC) as well as the Canada Foundation for Innovation (CFI). G.Q. acknowledges CNRS for a visiting position in Toulouse and support from EuroMagNET under EC Contract No. 506239.

[1] M. Fiebig, V. Pavlov, and R. Pisarev, J. Opt. Soc. Am. B **22**, 96 (2005).
[2] M. Fiebig, J. Phys. D **38**, R123 (2005).
[3] F. Yen, C. dela Cruz, B. Lorenz, E. Galstyan, Y. Sun, M. Gospodinov, and C. Chu, J. Mater. Res. **22**, 2163 (2007).
[4] D. Chiba, M. Sawicki, Y. Nishitani, Y. Nakatani, F. Matsukura, and H. Ohno, Nature (London) **455**, 515 (2008).
[5] Y. Zhang, Z. Li, C. Deng, J. Ma, Y. Lin, and C.-W. Nan, Appl. Phys. Lett. **92**, 152510 (2008).
[6] C. Binek and B. Doudin, J. Phys.: Condens. Matter **17**, L39 (2005).
[7] L. Martin, S. Crane, Y.-H. Chu, M. Holcomb, M. Gajek, M. Huijben, C.-H. Yang, N. Balke, and R. Ramesh, J. Phys.: Condens. Matter **20**, 434220 (2008).
[8] T. Kimura, T. Goto, H. Shintani, K. Ishizka, T. Arima, and Y. Tokura, Nature (London) **426**, 55 (2003).
[9] G. Lawes, A. B. Harris, T. Kimura, N. Rogado, R. J. Cava, A. Aharony, O. Entin-Wohlman, T. Yildirim, M. Kenzelmann, C. Broholm, and A. P. Ramirez, Phys. Rev. Lett. **95**, 087205 (2005).
[10] T. Kimura, J. C. Lashley, and A. P. Ramirez, Phys. Rev. B **73**, 220401(R) (2006).
[11] D. Lebeugle, D. Colson, A. Forget, M. Viret, P. Bonville, J. F. Marucco, and S. Fusil, Phys. Rev. B **76**, 024116 (2007).
[12] S. Mitsuda, M. Mase, K. Prokes, H. Kitazawa, and H. A. Katori, J. Phys. Soc. Jpn. **69**, 3513 (2000).
[13] O. A. Petrenko, G. Balakrishnan, M. R. Lees, D. M. Paul, and A. Hoser, Phys. Rev. B **62**, 8983 (2000).
[14] O. A. Petrenko, M. R. Lees, G. Balakrishnan, S. de Brion, and G. Chouteau, J. Phys.: Condens. Matter **17**, 2741 (2005).
[15] N. Terada, Y. Narumi, K. Katsumata, T. Yamamoto, U. Staub, K. Kindo, M. Hagiwara, Y. Tanaka, A. Kikkawa, H. Toyokawa, T. Fukui, R. Kanmuri, T. Ishikawa, and H. Kitamura, Phys. Rev. B **74**, 180404(R) (2006).
[16] H. Mitamura, S. Mitsuda, S. Kanetsuki, H. A. Katori, T. Sakakibara, and K. Kindo, J. Phys. Soc. Jpn. **76**, 094709 (2007).
[17] Y. Ajiro, T. Asano, T. Takagi, M. Mekata, H. A. Katori, and T. Goto, Physica B **201**, 71 (1994).
[18] S. Mitsuda, N. Kasahara, T. Uno, and M. Mase, J. Phys. Soc. Jpn. **67**, 4026 (1998).
[19] N. Terada, Y. Narumi, Y. Sawai, K. Katsumata, U. Staub, Y. Tanaka, A. Kikkawa, T. Fikui, K. Kindo, T. Yamamoto, R. Kanmuri, M. Hagiwara, H. Toyokawa, T. Ishikawa, and H. Kitamura, Phys. Rev. B **75**, 224411 (2007).
[20] M.-H. Whangbo, D. Dai, K.-S. Lee, and R. Kremer, Chem. Mater. **18**, 1268 (2006).
[21] G. Quirion, X. Han, M. L. Plumer, and M. Poirier, Phys. Rev. Lett. **97**, 077202 (2006).
[22] M. L. Plumer, K. Hood, and A. Caillé, Phys. Rev. Lett. **60**, 45 (1988).
[23] F. Ye, Y. Ren, Q. Huang, J. A. Fernandez-Baca, P. Dai, J. W. Lynn, and T. Kimura, Phys. Rev. B **73**, 220404(R) (2006).
[24] N. Terada, Y. Tanaka, Y. Tabata, K. Katsumata, A. Kikkawa, and S. Mitsuda, J. Phys. Soc. Jpn. **75**, 113702 (2006).
[25] G. Quirion, M. J. Tagore, M. L. Plumer, and O. A. Petrenko, Phys. Rev. B **77**, 094111 (2008).
[26] G. Quirion, M. J. Tagore, M. L. Plumer, and O. A. Petrenko, J. Phys. Conf. Ser. **145**, 012070 (2009).
[27] M. Mekata, N. Yaguchi, T. Takagi, T. Sugino, S. Mitsuda, H. Yoshizawa, N. Hosoito, and T. Shinjo, J. Phys. Soc. Jpn. **62**, 4474 (1993).
[28] T. Fukuda, H. Nojiri, M. Motokawa, T. Asano, M. Mekata, and Y. Ajiro, Physica B **246-247**, 569 (1998).
[29] F. Wang and A. Vishwanath, Phys. Rev. Lett. **100**, 077201 (2008).
[30] R. S. Fishman, F. Ye, J. A. Fernandez-Baca, J. T. Haraldsen, and T. Kimura, Phys. Rev. B **78**, 140407(R) (2008).
[31] M. L. Plumer, Phys. Rev. B **76**, 144411 (2007).
[32] M. L. Plumer, Phys. Rev. B **78**, 094402 (2008).
[33] B. Wolf, G. Bruls, I. Kouroudis, D. Finsterbusch, M. Sieling, S. Schmidt, W. Palme, and B. Lüthi, Physica B **246-247**, 179 (1998).
[34] S. Zherlitsyn, S. Schmidt, B. Wolf, H. Schwenk, B. Lüthi, H. Kageyama, K. Onizuka, Y. Ueda, and K. Ueda, Phys. Rev. B **62**, R6097 (2000).
[35] B. Wolf, S. Zherlitsyn, S. Schmidt, B. Lüthi, H. Kageyama, and Y. Ueda, Phys. Rev. Lett. **86**, 4847 (2001).
[36] B. Wolf, S. Zherlitsyn, H. Schwenk, S. Schmidt, and B. Lüthi, J. Magn. Magn. Mater. **226-230**, 107 (2001).
[37] B. Wolf, S. Zherlitsyn, S. Schmidt, and B. Lüthi, Phys. Status Solidi A **189**, 389 (2002).
[38] A. Suslov, J. B. Ketterson, D. G. Hinks, D. F. Agterberg, and B. K. Sarma, Phys. Rev. B **68**, 020406(R) (2003).
[39] M. F. Collins and O. A. Petrenko, Can. J. Phys. **75**, 605 (1997).